inter.noise
21-24 AUGUST
SCOTTISH EVENT CAMPUS
GLASGOW 2022

Modal Decomposition Analysis of Bluff-Body Stabilized Lean Premixed CH_4/H_2/air Flames Based on LES Data

Halit Kutkan[1]
University of Genoa
Via Montallegro, 1, 16145, Genoa, Italy

Alberto Amato[2]
Ansaldo Energia S.p.A.
Via Nicola Lorenzi, 8, 16152, Genoa, Italy

Giovanni Campa[3]
Ansaldo Energia S.p.A.
Via Nicola Lorenzi, 8, 16152, Genoa, Italy

Luis Tay-Wo-Chong[4]
Ansaldo Energia Switzerland AG
Haselstrasse, 18, 5401, Baden, Switzerland

ABSTRACT

Unsteady flow and flame dynamics of bluff body stabilized CH_4/H_2/air premixed flames are investigated numerically with LES and modal decomposition techniques. Energy ranked and frequency dependent modes are identified with proper orthogonal (POD), spectral proper orthogonal (SPOD) and dynamic mode decompositions (DMD). Flow and flame coherent structures are extracted based on the axial velocity and heat release rate (HRR) contours. Two cases, namely 100% CH_4/air (V-flame) and 43.4% CH_4 + 56.6% H_2/air (M-flame), are selected for the analysis. Each case is acoustically excited using large eddy simulation (LES) with harmonic excitation signal at a distinct frequency and with a broadband excitation signal to produce snapshots for modal decomposition analysis. In POD, the frequencies of the relevant modes are extracted with the discrete Fourier transform (DFT) of time coefficients, while in SPOD and DMD the extracted modes are frequency dependent by nature. Modal decomposition capabilities of the methods are tested by comparing the extracted modes from harmonic and broadband excited cases. Results are commented and capabilities of the methods are outlined.

[1] halit.kutkan@edu.unige.it

[2] alberto.amato@ansaldoenergia.com

[3] giovanni.campa@ansaldoenergia.com

[4] luis.taywochonghilares@ansaldoenergia.com

1. INTRODUCTION

Modal decomposition techniques are used in the literature to extract coherent structures in turbulent flow-field. These periodic structures are of interest due to being responsible for the dynamics of the system. Extracted mode shapes provide insight to system dynamics and could help to identify the sources of instabilities. POD (Proper Orthogonal Decomposition), SPOD (Spectral Proper Orthogonal Decomposition) and DMD (Dynamic Mode Decomposition) are the most common techniques, used for this purpose in the field of turbulence and combustion.

POD extracts spatially orthogonal and time independent energy ranked modes [1, 2]. This may result in merging of the modes of distinct frequencies in a single POD mode [3]. DMD provides temporally orthogonal modes, by associating a certain frequency and growth rate to each mode [2]. Depending on the sign of the growth rate, stability of the mode of interest is evaluated. However it does not rank the modes based on energies, hence the dominancy of the modes on the system dynamics is unknown. On the other hand, SPOD is referred as the frequency domain form of POD and provides spatially orthogonal modes that oscillate at a single distinct frequency. It preserves the energy ranking feature of POD and provides frequency dependent modes which correspond to the optimally averaged DMD modes [4] for statistically stationary flows. This feature provides superiority to SPOD over DMD in terms of extraction of the mode shapes and of the identification of the dominant modes. However, the growth rate, which defines the stability of the mode cannot be provided by SPOD, and in case of identifying the stability of the modes, DMD is of importance over SPOD.

In this study, modal decomposition analysis of 100%$_{vol}$ CH_4/air (with a V-flame topology) and 43.4%$_{vol}$ CH_4 + 56.6%$_{vol}$ H_2/air (with a M-flame topology) turbulent premixed flames is performed with POD, SPOD and DMD methods, and the capabilities of each method are outlined. Time resolved data is produced with acoustically excited LES and heat release rate and axial velocity contours on a section plane of a bluff body stabilized burner are recorded at a period of 0.00005 s. To test the methods' mode extraction capability, each case (V and M-flame) is excited with a harmonic excitation signal at a distinct frequency where the dominant mode frequency is known and with a broadband signal in white noise nature. Then the mode shapes, obtained from these cases are compared with each other.

The rest of the paper is organized as follows: In section 2, the LES data used for decomposition is explained, the applications of POD, SPOD and DMD methods on discrete set of LES data are explained in section 3, results are commented in section 4, and the paper is concluded with section 5.

2. LES DATA

The LES data used in this study was produced in a previous study [5]. LES simulations were performed on the laboratory scale bluff body stabilized single sector burner [6]. For the details of the combustion model and numerical setup, the reader is referred to [5]. LES cases are forced with one harmonic and one broadband velocity signal from the inlet. For the V-flame case (with 0% H_2) $f_{harm} = 200\ Hz$ is selected and for the M-flame case (with 56.6% H_2) $f_{harm} = 400\ Hz$ is selected for harmonic excitation signals. Broadband excitation signals are produced with TFDtools [7] as explained in [5] and presented in figure 1. Signal length is kept equal to 5000 time-steps for harmonic excitation, and to 10000 time-steps for broadband excitation, and the snapshots are recorded at every 5 time steps, forming 1000 snapshots for harmonic, and 2000 snapshots for broadband forced cases. In the production of the broadband signal, energy is uniformly distributed over the defined frequency range. As observed from PSD plots in figure 1, the range is limited up to 1000 Hz for the V-flame case, and up to 2000 Hz for the M-flame case. These ranges are selected based on the flames' cut-off frequencies, observed in the experiments [6].

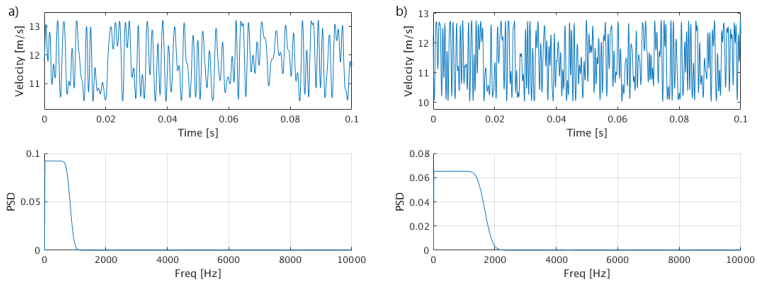

Figure 1: Broadband excitation signals a) for V-flame, b) for M-flame

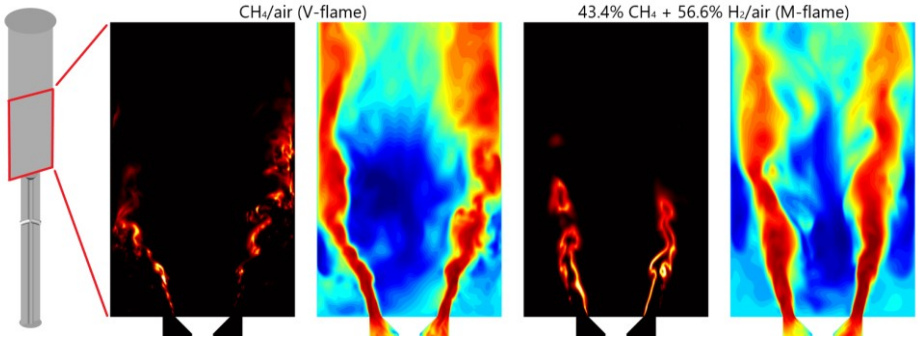

Figure 2: Instantaneous HRR and axial vel. contours plotted on the section plane for both flames

Instantaneous flame shapes and the axial velocities are depicted on the section plane for the two cases in figure 2. On the left in figure 2, three rods placed with 120° supporting the bluff body are shown. These rods cause asymmetric flame shapes on the section plane as more pronounced in the V-flame case.

3. MODAL DECOMPOSITION ANALYSIS

In the modal decomposition analyses carried out in this study, the recorded LES snapshots (HRR or axial velocity contours plotted on section plane) are downsized to the cartesian mesh size of 88x140 cells on the section plane by interpolation. Before applying modal decompositions, mean quantities are subtracted from instantaneous snapshots.

3.1. Proper Orthogonal Decomposition (POD)

Considering N_t as the number of snapshots, and M as the number of cells on the section plane, each snapshot can be written as a vector of M dimensions [4]. These snapshots are combined as the column vectors (s_i) of a data matrix $D = [s_1, s_2, \dots, s_{N_t}]$ with dimension of $M \times N_t$, and the correlation matrix, to be used in the eigenvalue problem, is formed as $C = D^*D$.

$$CW = \Lambda W \quad (1)$$

$$\Phi = DW\Lambda^{-1/2} \quad (2)$$

$$A = \Phi^* D \quad (3)$$

In Eq. (1) to (3) W, Λ, Φ and A refer to eigenvector matrix, eigenvalue matrix holding the eigenvalues on its diagonal, POD mode matrix holding modes as column vectors and amplitude matrix holding time coefficients as row wise vectors, respectively. And the superscript $*$ stands for the conjugate transpose. Dominant frequency of the extracted POD mode can be calculated by DFT transform of the regarding time coefficients. Eigenvalues over the diagonal of Λ matrix are placed in descending order, showing the dominancy of the related POD modes.

3.2. Spectral Proper Orthogonal Decomposition (SPOD)

In SPOD, before solving the eigenvalue problem, first the data matrix D is divided into N_{blk} number of block matrices B_i $(i = 1,2, \dots, N_{blk})$, following the well-known Welch's method [4, 8], provided that $N_t = N_{ovlp} + N_{blk}(N_{dft} - N_{ovlp})$. Each block B_i has N_{dft} number of column vectors by sharing N_{ovlp} number of column vectors with their neighbor blocks. Then each block is transformed into frequency domain with windowed DFT (Discrete Fourier Transform). Window function is used to prevent spectral leakages in the DFT transform, Hamming window can be used for this purpose which is also used in this study. Then, each block B_i is reorganized to have the column vectors from the same frequency, and each reorganized block $\hat{B}_i$ has N_{dft} number of column vectors as B_i. After this point, covariance matrix is constructed for SPOD as $C = \hat{B}_i^{\,*}\hat{B}_i$ and the eigenvalue problem is solved as in Eq. (1). Finally, the SPOD modes $\Phi_{SPOD,i}$ can be found as follows, similar to what done in POD.

$$\Phi_{SPOD,i} = \hat{B}_i W \Lambda^{-1/2} \tag{4}$$

Frequencies belonging to SPOD modes are evaluated as follows:

$$\begin{aligned} f_i &= (i-1)/N_{dft}\Delta t \qquad i \le N_{dft}/2 \\ f_i &= \left(i-1-N_{dft}\right)/N_{dft}\Delta t \qquad i > N_{dft}/2 \end{aligned} \tag{5}$$

3.3. Dynamic Mode Decomposition (DMD)

Application of DMD requires input and output matrices which can be formed as $X = [s_1, s_2, \dots, s_{N_t-1}]$ and $X' = [s_2, s_3, \dots, s_{N_t}]$. The first step is to take the singular value decomposition of the input matrix:

$$X = U\Sigma V^* \tag{6}$$

Where U and V are the left and right singular vector matrices of X, and Σ is the singular value matrix holding singular values on its diagonal. Assuming linear relation between input and output matrices as $X' = RX$, and using Eq. (6), R can be expressed as [9]:

$$R = X'V\Sigma^{-1}U^* \tag{7}$$

Then the projection of the R matrix onto left eigenvector matrix is done as follows:

$$\tilde{R} = U^*X'V\Sigma^{-1} \tag{8}$$

and the eigenvalue problem is solved for the projection matrix $\tilde{R}$.

$$\tilde{R}W = \Lambda W \tag{9}$$

In the end, DMD modes are found as follows:

$$\Phi_{DMD} = X'V\Sigma^{-1}W = UW \tag{10}$$

with frequency and growth rate of each mode are evaluated as below:

$$\begin{aligned} f_i &= Im[ln(\lambda_{DMD,i})/2\pi\Delta t] \\ \sigma_i &= Re[ln(\lambda_{DMD,i})/\Delta t] \end{aligned} \tag{11}$$

where λ_i are the eigenvalues, calculated with Eq. (9) and Δt is the time step between the sampled snapshots.

4. RESULTS

Figure 3 shows the extracted mode shapes from harmonically excited cases for both V and M-flames. For POD the most dominant modes are plotted, for SPOD and DMD, the modes at the excitation frequencies ($f = 200\ Hz$ and $f = 400\ Hz$) are plotted. All three methods captured similar mode shapes. Despite some discrepancies in the V-flame case, very similar structures are observed for the M-flame case. The more compact M-flame provided more significant mode shapes than the V-flame. SPOD and DMD modes matched well with each other for both V and M-flames. Although

HRR POD mode for V-flame showed some discrepancies, reasonable agreement is achieved. Similarity of the mode shapes suggests that POD is able to capture the mode shape of a single frequency under harmonic excitation.

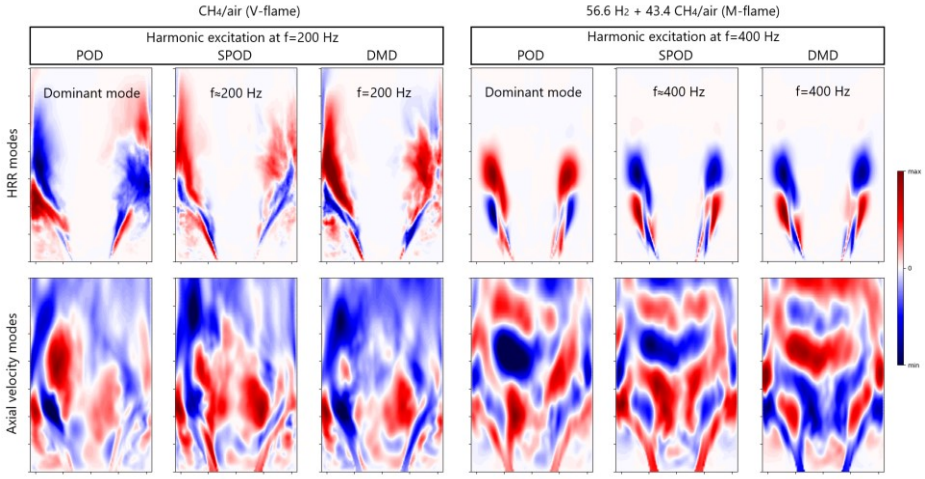

Figure 3: Extracted mode shapes with POD, SPOD and DMD for V and M-flames under harmonic excitations.

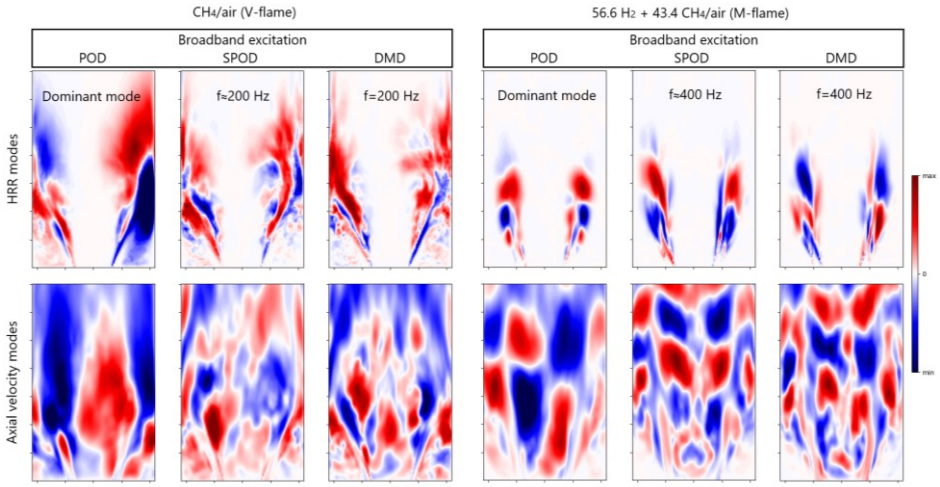

Figure 4: Extracted mode shapes with POD, SPOD and DMD for V and M-flames under broadband excitations.

In figure 4, extracted mode shapes from broadband excited cases are shown. Similar to figure 3, the most dominant mode shapes are plotted for POD. In order to compare the modes with those from harmonically excited cases, the mode shapes at the harmonic excitation frequencies are plotted for SPOD and DMD. As observed, the extracted POD modes are different than those from the SPOD and DMD this time. On the other hand, SPOD and DMD modes are similar to each other. Comparing SPOD and DMD modes from figures 3 and 4, shows that both methods are capable of extracting correct mode shapes at a particular frequency, even if they are not excited for it.

Unlike the case with harmonic excitation, the dominant POD mode in figure 4 is the combined mode of different frequencies, rather than being a mode of single distinct frequency. To identify these

frequencies, DFT of the time coefficients of these dominant POD modes (shown in figure 3 and 4) is plotted in figure 5. Since POD provides spatially orthogonal energy ranked modes, frequency relevant information is obtained by the DFT transform of the extracted mode's time coefficients. On the other hand, in SPOD, the modes are extracted with already associated frequencies.

Figure 5 compares the SPOD eigenvalue plots with the DFT of the dominant POD mode time coefficients. In SPOD eigenvalue plots (the first and the third row in figure 5), the curves with the highest energy (blue curves) refer to the leading (the most dominant) modes, and the others refer to the other modes up to N_{blk}'th mode with energies in descending order.

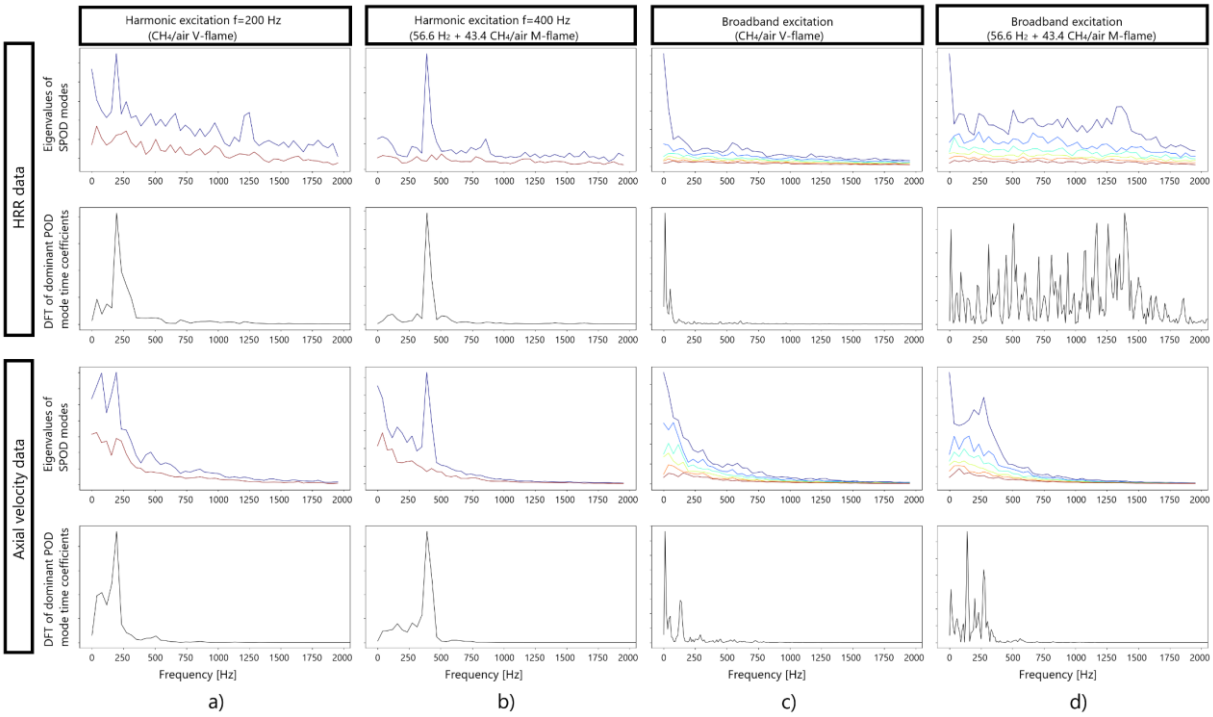

Figure 5: DFT of the most dominant POD mode time coefficients and the SPOD eigenvalues for V and M-flames under harmonic and broadband excitations.

In harmonic excitation cases (Figure 5a and 5b), the peaks are observed at the harmonic excitation frequencies. The peaks at the DFT plots (the second and fourth rows in figure 5a and 5b) validate that the dominant POD modes, extracted in figure 3, are the modes of the harmonic excitation frequencies (200 Hz and 400 Hz). Similarly, SPOD eigenvalue plots (the first and third rows in figure 5a and 5b) show the highest energy peaks at these harmonic excitation frequencies. On the other hand, in broadband excitation cases, the peaks are distributed in range of frequencies. Comparing figures 1a and 1b to figures 5c and 5d shows that the frequency distribution ranges of the peaks are similar to those in broadband excitation signal, proving that POD and SPOD can predict the dominant frequencies of the system. While POD captures the dominant frequencies embedded in a single mode, SPOD captures the modes at each frequency separately and evaluates their energies based on their eigenvalues.

The peaks in the DFT plots (the second and fourth rows in figure 5c and 5d) show that the dominant POD modes, extracted in figure 4, are the combined mode of the peak frequencies. Figure 5c and 5d (the first and third rows) also show that HRR reflects more the effect of excitation than axial velocity, as its distributed peaks recover the broadband excitation range better.

Another observation from HRR SPOD eigenvalues plot (the first row of figures 5c and 5d) is that compact M-flame responds the acoustic excitation more than V-flame, as the M-flame peak amplitudes in the excitation range are more significant than those of V-flame. The ratio of flame surface area change to total flame surface area is less in longer V-flame than in M-flame, causes lower response. As previously mentioned, also the mode shapes of M-flame are more significant.

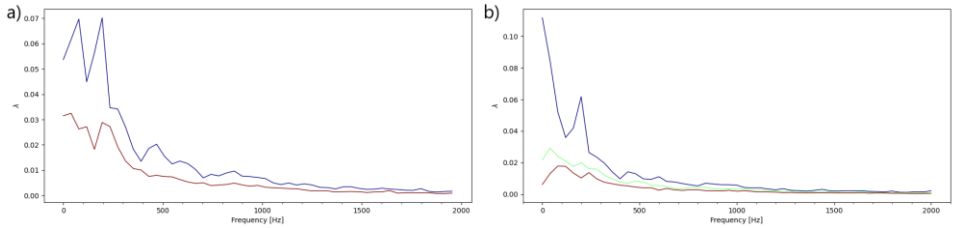

Figure 6: SPOD eigenvalues of axial velocity of V-flame harmonic excitation case, a) with $N_{fft} = 512$ and $N_{ovlp} = 256$, b) with $N_{fft} = 500$ and $N_{ovlp} = 250$

Figure 6 is plotted to show that the peak around 100 Hz (the third row figure in 5a), seen in the SPOD eigenvalues plots for V-flame harmonic excitation case, is due to the spectral leakage occurred in the application of Welch's method in SPOD. This may happen in the application of SPOD depending on the selected N_{fft} and N_{ovlp} parameters and on the number of snapshots. Figure 6 is plotted to show that the peak disappears when the $N_{fft} = 500$ with $N_{ovlp} = 250$ are chosen instead of $N_{fft} = 512$ with $N_{ovlp} = 256$.

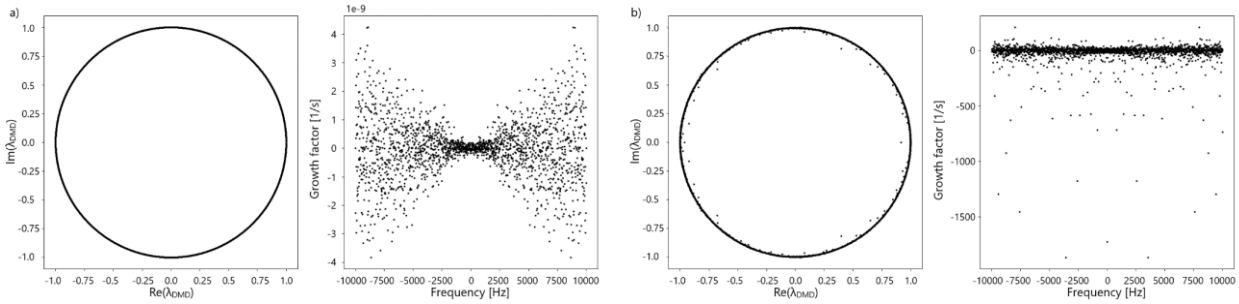

Figure 7: DMD eigenvalues and growth rates of HRR for M-flame broadband excitation case a) DMD with mean subtraction, b) DMD without mean subtraction

In figure 7, DMD eigenvalues and growth rates are plotted with and without mean subtraction from the snapshots data. Different from POD and SPOD, DMD eigenvalues provide information on the stability of belonging modes, rather than providing information of mode energies. In the case of mean subtraction, the complex valued eigenvalues are placed over the unit circle (see figure 7a), hence their growth rates converge to zero (max growth rate value is in the range of 1e-9 1/s). In the case of without mean subtraction, the eigenvalues are scattered over the region close to unit circle (see figure 7b), and their growth rates take either positive (growth rate, unstable mode) or negative value (decay rate, stable mode), which provides information about the stability of the regarding modes.

5. CONCLUSIONS

Modal decomposition analysis of acoustically excited CH_4/H_2/air premixed flames was performed with POD, SPOD and DMD techniques on LES data. Two mixtures CH_4/air (V-flame) and 43.4%

CH_4 + 56.6% H_2/air (M-flame) were selected for the analysis and each case was excited with harmonic and broadband excitation signals to produce snapshots. Mode extraction capabilities were tested qualitatively, by comparing the extracted mode shapes from three decomposition techniques under harmonic and broadband excitations. For POD, the dominant mode is extracted, and for SPOD and DMD, the modes at the harmonic excitation frequencies are extracted. In harmonic excitations all three methods captured the dominant mode of excitation frequency. However, in broadband excitations, only SPOD and DMD could capture the regarding harmonic mode, while POD captured the combined mode instead. DFT of the extracted POD mode's time coefficients were plotted in comparison with SPOD eigenvalues, and it was shown that, both methods could identify the dominant frequencies of the system under both harmonic and broadband forcing conditions. DMD eigenvalues are plotted for the HRR data from M-flame under broadband forcing. It is shown that, in order to have information about the stability of the modes, DMD should be applied on the data without mean subtraction.

SPOD and DMD with mean subtraction are found to be capable of extraction of correct mode shapes at different frequencies although they are not forced exclusively. In terms of extracting the mode shapes, SPOD and DMD provided very similar coherent structures and any of them can be preferred to the other. However, for better identifying the dynamics of turbulent flame and flow-field, SPOD and DMD are suggested to be used together, as one provides information on the mode dominancy, and the other provides information on the mode stability. On the other hand, for such a purpose, SPOD eliminates the requirement of the POD usage.

6. ACKNOWLEDGEMENTS

This work is part of the Marie Skłodowska-Curie Initial Training Network Pollution Know-How and Abatement (POLKA). The authors gratefully acknowledge the financial support from the European Commission under call H2020-MSCA-ITN-2018 (project number: 813367).

7. REFERENCES

[1] Schmidt O. T. & Towne A., "An efficient streaming algorithm for spectral proper orthogonal decomposition," *Computer Physics Communications*, **237**, 98–109, (2019).

[2] Brouzet D., Haghiri A., Talei M., Brear M. J., Schmidt O. T., Rigas G., & Colonius T., "Role of coherent structures in turbulent premixed flame acoustics," *AIAA Journal*, **58(6)**, 2635–2642, (2020).

[3] Sieber M., Paschereit C. O. & Oberleithner K., "Advanced identification of coherent structures in swirl-stabilized combustors," *Journal of Engineering for Gas Turbines and Power*, **139(2)**, (2017).

[4] Towne A., Schmidt O. T. & Colonius T., "Spectral proper orthogonal decomposition and its relationship to dynamic mode decomposition and resolvent analysis," *J. Fluid Mech.*, **847**, 821–867, (2018).

[5] Kutkan H., Amato A., Campa G., Tay-Wo-Chong L. & Æsøy E., "LES of turbulent premixed CH_4/H_2/air flames with stretch and heat loss for flame characteristics and dynamics," *Proceedings of ASME Turbo Expo GT2022*, p. 13., Rotterdam, The Netherlands, June 2022.

[6] Æsøy E., Aguilar J. G., Bothien M. R., Worth N. A., & Dawson J. R., "Acoustic-convective interference in transfer functions of methane/hydrogen and pure hydrogen flames.," *Journal of Engineering for Gas Turbines and Power*, **143(12)**, (2021).

[7] Huber A. & Polifke W., "Dynamics of practical premixed flames, part I: model structure and identification," *International Journal of Spray and Combustion Dynamics*, **1(2)**, 199–228, (2009).

[8] Schmidt O. T. & Colonius T., "Guide to spectral proper orthogonal decomposition," *AIAA Journal*, **58(3)**, 1023–1033, (2020).

[9] Peng J., Gao L., Yu X., Qin F., Liu B., Cao Z., Wu G. & Han M., "Combustion oscillation characteristics of a supersonic ethylene jet flame using high-speed planar laser-induced fluorescence and dynamic mode decomposition," *Energy*, **239**, (2022).